

Magnetic and Transport Properties of the Kondo Lattice Compound YbPtAs *

Hui Liang(梁慧)^{1,2}, Shuai Zhang(张帅)¹, Yu-Jia Long(龙雨佳)¹, Jun-Bao He(何俊宝)¹, Jing Li(李婧)^{1,2},
Xin-Min Wang(王欣敏)^{1,2}, Zhi-An Ren(任治安)^{1,2,3}, Gen-Fu Chen(陈根富)^{1,2,3}

¹*Institute of Physics and Beijing National Laboratory for Condensed Matter Physics,
Chinese Academy of Sciences, Beijing 100190*

²*School of Physical Sciences, University of Chinese Academy of Sciences, Beijing 100049*

³*Collaborative Innovation Center of Quantum Matter, Beijing 100190*

(Received 2 May 2018)

We report the electrical resistivity, magnetic susceptibility, and heat capacity studies on a new intermetallic compound YbPtAs, which crystallizes in a modified AlB₂ type structure. The Yb ions in YbPtAs are in a trivalent state and order antiferromagnetically around Néel temperatures $T_{N1} = 6.5$ K and $T_{N2} = 2.2$ K, respectively, deduced both from the magnetic susceptibility $\chi(T)$ and heat capacity $C(T)$ measurements. The magnetic contribution in resistivity, $\rho_m(T)$, exhibits a broad maximum at around 100 K and a logarithmic temperature dependence in the high-temperature region, indicative of the presence of the Kondo effect in YbPtAs.

PACS: 75.30.Mb, 71.27.+a, 75.30.Cr, 75.20.Hr

DOI: 10.1088/0256-307X/35/7/077503

Transition metal pnictides have attracted considerable attention owing to their peculiar electronic and magnetic properties.^[1–9] The discovery of high-temperature superconductivity in iron pnictides raised the hopes of setting a new T_c record^[1–3] and the possibility of an unconventional superconducting mechanism.^[10–12] Very recently, SrPtAs, crystallizing in a hexagonal AlB₂-type structure, was reported to be a new novel superconductor with some unconventional superconducting states, which is strongly related to the local lack of inversion symmetry of the two distinct conducting layers in the unit cell of SrPtAs.^[4,13–15] MgB₂ is another well-known high- T_c superconductor with the same AlB₂-type structure.^[16] In the ternary system AMX (A: alkaline-earth; M: transition metal; X: pnictogen) with the AlB₂ structure such as SrPtAs, alkaline-earth cations occupy the Al sites, while transition metal and pnictogen take the position of the boron atoms forming hexagonal layers.

On the other hand, upon the substitution of alkaline-earth with rare-earth metals, the ternary AMX monopnictides also show a rich variety of unconventional phenomena: such as the Kondo insulating state in CeRhAs,^[5,17–19] the topological superconductivity in YPtBi^[8,20] and LuPtBi,^[7,21] and the Weyl fermions in GdPtBi.^[9] However, these compounds crystallize with different structure types. For the diverse physical properties shown in ternary rare Earth pnictides, these materials are appropriate candidates to study these novel quantum phenomena. Strangely, a few decades ago, YbPtAs^[22,23] was reported to crystallize in an AlB₂ derived hexagonal structure, the same as SrPtAs, but there has been little study on the physical properties. In this case, the substitution of Sr with Yb would introduce a localized

moment from 4*f* electrons, and the hybridization between the localized 4*f*-electrons and conduction electrons can produce exotic properties, like the heavy fermion superconductivity.

In this Letter, we report a systematic experimental study on polycrystalline samples of YbPtAs. Powder x-ray diffraction (XRD) is used to verify the structure. The magnetic susceptibility, electrical resistivity, and heat capacity of YbPtAs are measured at temperatures down to 1.8 K under different fields. To study the contribution of 4*f* electrons, LuPtAs is investigated as a reference material. Two antiferromagnetic (AFM) transitions related to Yb³⁺ ions are confirmed in magnetic and heat capacity measurements. The hump in electrical resistivity strongly implies the presence of the Kondo coherence.

In the experiment, the polycrystalline sample of YbPtAs was prepared using a solid state reaction method. The starting materials Yb, Pt, and As were mixed together at a molar ratio of 1:1:1 under a high purity argon atmosphere in a glove box. The mixture was pressed into pellets and sealed into an evacuated quartz tube, which was heated at 1000°C for 50 h, followed by a natural cooling down. To characterize the structure, XRD with Cu K_α radiation was carried out at ambient temperature. Magnetic measurements were performed on a quantum design magnetic property measurement system (MPMS). Resistivity and specific heat were measured in a quantum design physical property measurement system (PPMS).

The powder XRD pattern of the as-prepared YbPtAs is shown in Fig. 1. To obtain the crystal structure and lattice constant, Rietveld refinement has been performed using the GSAS program. The black solid line shows the calculated pattern and the red dots show

*Supported by the National Basic Research Program of China under Grant No 2015CB921303, the National Key Research Program of China under Grant No 2016YFA0300604, the Strategic Priority Research Program (B) of Chinese Academy of Sciences under Grant No XDB07020100, and the National Natural Science Foundation of China under Grant No 11404175.

**Corresponding author. Email: gfchen@iphy.ac.cn

© 2018 Chinese Physical Society and IOP Publishing Ltd

the observed data. The main peaks are indexed well to a hexagonal AlB_2 -type structure with space group $P63/mmc$ (No. 194). The lattice parameters derived from the Rietveld analysis are $a = b = 4.234(2)$ Å and $c = 14.84(1)$ Å, which are coincident with those reported in the literature.^[22,23] The insets indicate the hexagonal structure of YbPtAs and the alternating layers of Yb and PtAs hexagon could be seen clearly along the c -axis in the right inset.

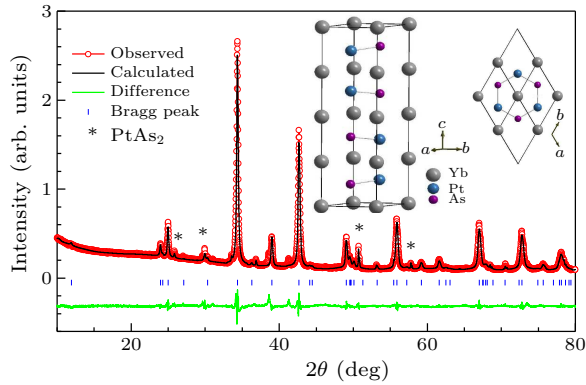


Fig. 1. Typical results of Rietveld refinement with GSAS for the YbPtAs XRD pattern. The insets are the crystal structures of YbPtAs viewed along different directions.

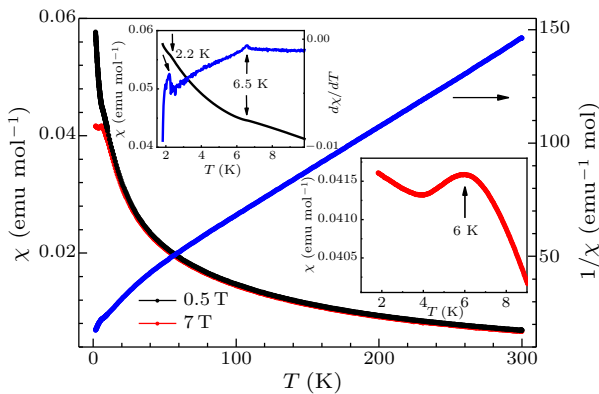


Fig. 2. Magnetic susceptibility versus temperature of YbPtAs at magnetic field $\mu_0 H = 0.5$ T and 7 T, respectively. The blue line presents the inverse magnetic susceptibility $1/\chi$ and the good fitting with the Curie-Weiss law for $T > 100$ K. The upper left inset shows the enlarged plot and the corresponding differential curve for $\mu_0 H = 0.5$ T. The lower right inset is the enlarged plot of $\chi(T)$ at $\mu_0 H = 7$ T and $T < 10$ K.

In Fig. 2, the lines in black and red are the susceptibility χ as a function of temperature T measured under the magnetic field $\mu_0 H = 0.5$ T and 7 T, respectively. The upper left inset shows the enlarged plot of χ - T (red) and the corresponding differential curve (blue) measured at $\mu_0 H = 0.5$ T below 10 K. Two anomalies at 2.2 K and 6.5 K are observed, indicating AFM ordering and the two Néel temperatures are $T_{N1} = 6.5$ K and $T_{N2} = 2.2$ K. The lower right inset is the enlarged view of χ - T for $\mu_0 H = 7$ T. As the increase of magnetic field, the first AFM transition is suppressed to 6 K and the second AFM transition could not be observed down to 1.8 K. The blue line is

the inverse magnetic susceptibility versus temperature for $\mu_0 H = 0.5$ T. The $\chi(T)$ data above $T = 100$ K exhibits good Curie-Weiss behavior, and can be well fitted to $\chi = \chi_0 + C/(T - \theta_p)$, the value of paramagnetic Curie temperature θ_p is -65 K indicating AFM correlations. The Curie constant $C = 2.58$ emu·K·mol $^{-1}$ corresponds to the effective magnetic moment $\mu_{\text{eff}} = 4.51\mu_B$, which is very close to the value expected for the free Yb $^{3+}$ ion, $4.54\mu_B$, indicating that the Yb ion is primarily in a $4f^{13}$ configuration in this compound. Below 100 K, $1/\chi(T)$ shows a slight curvature, which is very likely due to crystal-electric-field (CEF) effects.

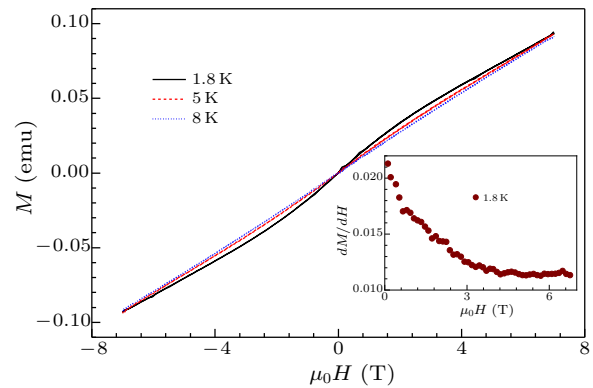


Fig. 3. Isothermal magnetization as a function of applied magnetic field at 1.8 K, 5 K, and 8 K. The inset is the derivative of magnetization for $\mu_0 H \geq 0$ T.

Figure 3 shows the isothermal $M(H)$ of YbPtAs for $|\mu_0 H| \leq 7$ T at the selected temperatures of 1.8 K, 5 K, and 8 K. The isothermal $M(H)$ at 8 K is almost linear while below T_{N1} , at 1.8 K and 5 K, isothermal $M(H)$ shows nonlinear behavior. The inset shows the behavior of dM/dH versus $\mu_0 H$ for $T = 1.8$ K. The slope decreases gradually with increasing the field as shown in the dM/dH curve and the noteworthy feature in the $M(H)$ curve shows a tendency towards saturation. This feature appears to be a metamagnetic transition induced by the magnetic field.^[24–26]

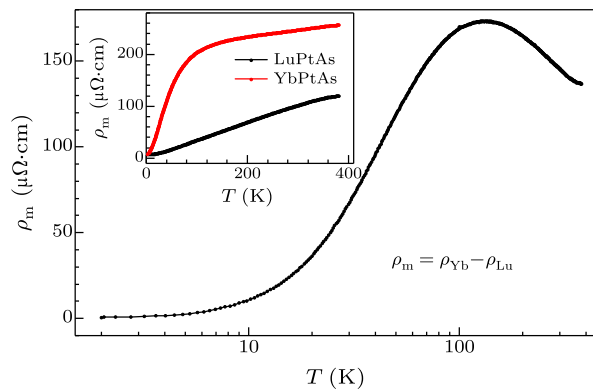


Fig. 4. Temperature dependence of electrical resistance of YbPtAs. Here ρ_m is the contribution of $4f$ electrons obtained by subtracting the resistivity of LuPtAs from that of YbPtAs. The red and blue lines in the inset are the resistivities of YbPtAs and LuPtAs, respectively.

The transport properties of YbPtAs and LuPtAs

are depicted in Fig. 4. The inset presents the temperature dependence of resistivity of YbPtAs and LuPtAs, respectively. The $4f$ -orbitals in LuPtAs are completely filled, and the hybridization of $4f$ -electrons with conduction electrons is expected to be too small to affect the electronic properties in LuPtAs. Here we use LuPtAs as a reference material to extract magnetic and electronic properties of YbPtAs caused by $4f$ -electrons. At high temperature, the resistivity of YbPtAs decreases linearly as a conventional metal. In contrast to LuPtAs, a prominent decrease from the linear behavior was observed in the ρ - T curve at about 100 K. This is a distinct feature of the Kondo lattice system and could be interpreted as the onset of the coherent Kondo scattering on account of the hybridization between the localized $4f$ and the conduction electrons. If one subtracts the resistivity of non-magnetic LuPtAs to get rid of the phonon contribution, i.e., $\rho_m = \rho_{\text{YbPtAs}} - \rho_{\text{LuPtAs}}$, a broad peak around 100 K, and a logarithmic temperature dependence in the high temperature regions are clearly observed in $\rho_m(T)$, resembling the temperature dependence of $\rho(T)$ of the heavy-fermion compounds.^[28–30]

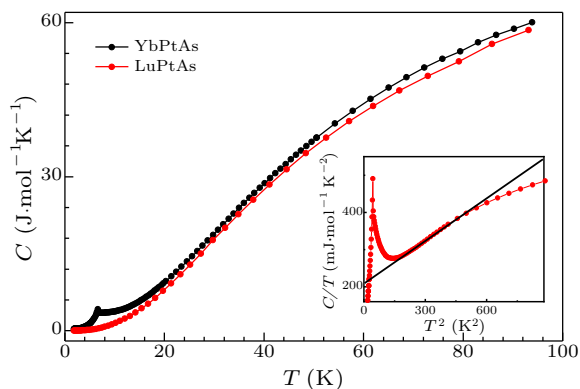


Fig. 5. Temperature dependences of specific heat are plotted for YbPtAs (red) and LuPtAs (blue), respectively. The obvious anomaly is observed at 6.6 K in YbPtAs data. The inset shows an enlarged view of the YbPtAs curve and γ derived from extrapolating the C - T plot.

Figure 5 presents the heat capacity C as a function of temperature T . The red curve is for YbPtAs and the blue one is for LuPtAs. At high temperature, the heat capacity in YbPtAs reduces with decreasing temperature, which is the same as that of LuPtAs. However, a distinct anomaly is observed at 6.6 K for YbPtAs, which is consistent with the transition in susceptibility, indicating the second order transition arising from the occurrence of AFM. The inset shows the enlarged plot of YbPtAs below 30 K. Another anomaly is observed at 2.2 K in accordance with the abnormal of magnetic susceptibility, which is rather small compared with the first transition of 6.6 K. To exclude this anomaly arising from the impurity phase, we have tried to prepare the single crystals, but the obtained crystals are very small. The heat capacity obtained by measuring about twenty single crystals simultaneously shows the same rise at 2.2 K, which demon-

strates clearly that the second anomaly is an intrinsic characteristic of YbPtAs and excludes the contribution of impurity. The crystal structure of YbPtAs has inequivalent Pt-As layers as shown in Fig. 1; this local inversion symmetry breaking has an effect on the Yb^{3+} ions and may yield two AFM phases. In the normal state, the specific heat capacity C can be written as

$$C = \gamma T + \beta T^3 + \delta T^5,$$

where γT is the contribution of electronic heat capacity C_e , and $\beta T^3 + \delta T^5$ is the common low temperature approximation for the lattice heat capacity C_l . A fit of the data to the formula yields the Sommerfeld coefficient $\gamma = 3.4 \text{ mJ}\cdot\text{mol}^{-1}\text{K}^{-2}$ for LuPtAs (not shown). As shown in the inset, the Sommerfeld value of YbPtAs obtained from an extrapolation of the T^2 dependence gives $\gamma = 213 \text{ mJ}\cdot\text{mol}^{-1}\text{K}^{-2}$. The Sommerfeld coefficient for YbPtAs is nearly 70 times larger than that of LuPtAs, indicating the correlated effect contributed from $4f$ electrons.

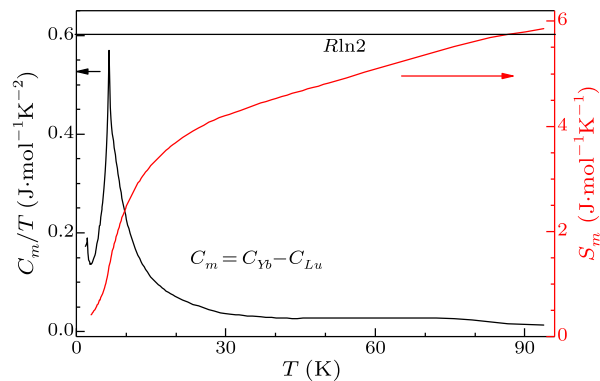


Fig. 6. The magnetic specific heat C_m/T arising due to $4f$ electrons versus T . To the right, the magnetic entropy gain calculated from magnetic specific heat data.

Since YbPtAs and LuPtAs have almost the same phonon contribution, the $4f$ electron contribution to the specific heat C_m was calculated by subtracting the specific heat of LuPtAs from the specific heat of YbPtAs as shown in Fig. 6. Two obvious λ type anomalies in C_m at 6.6 K and 2.2 K can be clearly observed. The magnetic entropy S_m calculated by integrating C_m/T over temperature is present in Fig. 6. The magnetic entropy reaches $0.6R \ln 2$ at about 15 K, which is far lower than the twofold degeneracy, a Kramers doublet. Here S_m is close to $R \ln 2$ at 90 K. The reduced magnetic entropy may result from the Kondo interactions that partially destroyed the degeneracy of the doublet ground state and the short range order above T_{N1} .^[31,32]

In summary, we have prepared polycrystalline YbPtAs samples and investigated the magnetization, resistivity, and specific heat properties. YbPtAs is confirmed to be a new compound of the AFM Kondo lattice. The Kondo coherent behavior appeared in $\rho(T)$ and two successive AFM transitions of Yb^{3+} ions have been observed at $T_{N1} = 6.5 \text{ K}$ and $T_{N2} =$

2.2 K, respectively. The obtained effective moment $\mu_{\text{eff}} = 4.51\mu_{\text{B}}$ and the Sommerfeld coefficient $\gamma = 213 \text{ mJ}\cdot\text{mol}^{-1}\text{K}^{-2}$ are due to the contribution from $4f$ electrons.

References

- [1] Kamihara Y, Watanabe T, Hirano M and Hosono H 2008 *J. Am. Chem. Soc.* **130** 3296
- [2] Chen G F, Li Z, Wu D, Li G, Hu W Z, Dong J, Zheng P, Luo J L and Wang N L 2008 *Phys. Rev. Lett.* **100** 247002
- [3] Ren Z A, Lu W, Yang J, Yi W, Shen X L, Zheng C, Che G C, Dong X L, Sun L L, Zhou F and Zhao Z X 2008 *Chin. Phys. Lett.* **25** 2215
- [4] Nishikubo Y, Kudo K and Nohara M 2011 *J. Phys. Soc. Jpn.* **80** 055002
- [5] Kumigashira H, Sato T, Yokoya T, Takahashi T, Yoshii S and Kasaya M 1999 *Phys. Rev. Lett.* **82** 1943
- [6] Goll G, Marz M, Hamann A, Tomanic T, Grube K, Yoshino T and Takabatake T 2008 *Physica B* **403** 1065
- [7] Tafti F, Fujii T, Juneau-Fecteau A, de Cotret S R, Doiron-Leyraud N, Asamitsu A and Taillefer L 2013 *Phys. Rev. B* **87** 184504
- [8] Butch N P, Syers P, Kirshenbaum K, Hope A P and Paglione J 2011 *Phys. Rev. B* **84** 220504
- [9] Hirschberger M, Kushwaha S, Wang Z, Gibson Q, Liang S, Belvin C A, Bernevig B, Cava R and Ong N 2016 *Nat. Mater.* **15** 1161
- [10] Paglione J and Greene R L 2010 *Nat. Phys.* **6** 645
- [11] Johnston D C 2010 *Adv. Phys.* **59** 803
- [12] Hirschfeld P, Korshunov M and Mazin I 2011 *Rep. Prog. Phys.* **74** 124508
- [13] Goryo J, Fischer M H and Sigrist M 2012 *Phys. Rev. B* **86** 100507
- [14] Biswas P K, Luetkens H, Neupert T, Stürzer T, Baines C, Pascua G, Schnyder A P, Fischer M H, Goryo J, Lees M R et al 2013 *Phys. Rev. B* **87** 180503
- [15] Fischer M H, Neupert T, Platt C, Schnyder A P, Hanke W, Goryo J, Thomale R and Sigrist M 2014 *Phys. Rev. B* **89** 020509
- [16] Nagamatsu J, Nakagawa N, Muranaka T, Zenitani Y and Akimitsu J 2001 *Nature* **410** 63
- [17] Kumigashira H, Takahashi T, Yoshii S and Kasaya M 2001 *Phys. Rev. Lett.* **87** 067206
- [18] Sasakawa T, Suemitsu T, Takabatake T, Bando Y, Umeo K, Jung M, Sera M, Suzuki T, Fujita T, Nakajima M et al 2002 *Phys. Rev. B* **66** 041103
- [19] Takabatake T, Sasakawa T, Kitagawa J, Suemitsu T, Echizen Y, Umeo K, Sera M and Bando Y 2003 *Physica B* **328** 53
- [20] Bay T V, Naka T, Huang Y K and de Visser A 2012 *Phys. Rev. B* **86** 064515
- [21] Pavlosiuk O, Kaczorowski D and Wiśniewski P 2015 *Sci. Rep.* **5** 9158
- [22] Wenski G and Mewis A 1986 *Z. Kristallogr.-Cryst. Mater.* **176** 125
- [23] Kuss M, Wenski G, Mewis A and Schuster H U 1987 *Z. Anorg. Allg. Chem.* **553** 156
- [24] Yamada H 1993 *Phys. Rev. B* **47** 11211
- [25] Millis A J, Schofield A J, Lonzarich G G and Grigera S A 2002 *Phys. Rev. Lett.* **88** 217204
- [26] Tokiwa Y, Pikul A, Gegenwart P, Steglich F, Bud'ko S L and Canfield P C 2006 *Phys. Rev. B* **73** 094435
- [27] Kaga H, Kubo H and Fujiwara T 1988 *Phys. Rev. B* **37** 341
- [28] Schilling J S 1986 *Phys. Rev. B* **33** 1667
- [29] Lee W H, Kwan K S, Klavins P and Shelton R N 1990 *Phys. Rev. B* **42** 6542
- [30] Ślebarski A and Spalek J 2005 *Phys. Rev. Lett.* **95** 046402
- [31] Bredl C D, Steglich F and Schotte K D 1978 *Z. Phys. B: Condens. Matter* **29** 327
- [32] Huo D, Sakurai J, Kuwai T, Mizushima T and Isikawa Y 2002 *Phys. Rev. B* **65** 144450